REPORT DOCUMENTATION PAGE

Form Approved
OMB No. 0704-0188

1. REPORT DATE *(DD-MM-YYYY)*	2. REPORT TYPE	3. DATES COVERED *(From - To)*
26-01-2010	Final Performance Report	01/04/2007-30/11/2009

4. TITLE AND SUBTITLE
Hadamard Transform Time-of-Flight Spectroscopy

5a. CONTRACT NUMBER

5b. GRANT NUMBER
FA9550-07-1-0316

5c. PROGRAM ELEMENT NUMBER

6. AUTHOR(S)
Richard N. Zare
Matthew D. Robbins
Griffin K. Barbula
Richard Perry

5d. PROJECT NUMBER

5e. TASK NUMBER

5f. WORK UNIT NUMBER

7. PERFORMING ORGANIZATION NAME(S) AND ADDRESS(ES)
Department of Chemistry
Stanford University
Stanford, CA 94305-5080

8. PERFORMING ORGANIZATION REPORT NUMBER

9. SPONSORING / MONITORING AGENCY NAME(S) AND ADDRESS(ES)
Air Force Office of
Scientific Research
4015 Wilson Blvd.
Room 713
Arlington, VA 22203-1954

10. SPONSOR/MONITOR'S ACRONYM(S)
AFOSR

11. SPONSOR/MONITOR'S REPORT NUMBER(S)
AFRL-OSR-VA-TR-2012-0439

12. DISTRIBUTION / AVAILABILITY STATEMENT
Distribution A: Approved for Public Release

13. SUPPLEMENTARY NOTES
None

14. ABSTRACT
This report describes the implementation of a new form of time-of-flight mass spectrometry based upon beam modulation and imaging detection which can be applied to studies of continuous ion beams requiring fast data acquisition rates over a large mass-to-charge ratio range. In addition, the use of the imaging detector in this method allows collection of mass-to-charge resolved movies of an ion beam. The capabilities of this method are demonstrated in studies of ion fragmentation reactions, biochemical kinetics, and the fundamental limitations of desorption electrospray ionization.

15. SUBJECT TERMS
Mass spectrometry, Bradbury-Nielsen Gates, Hadamard Transform, DESI, Kinetics, Trypsin, Stopped-Flow, Surface-Induced Dissociation

16. SECURITY CLASSIFICATION OF:			17. LIMITATION OF ABSTRACT	18. NUMBER OF PAGES	19a. NAME OF RESPONSIBLE PERSON
a. REPORT	b. ABSTRACT	c. THIS PAGE		40	Michael Berman
					19b. TELEPHONE NUMBER *(include area code)* (703) 696-7781

FINAL PERFORMANCE REPORT

TITLE: Hadamard Transform Time-of-Flight Mass Spectrometry

GRANT NUMBER: FA9550-07-1-0316

PRINCIPAL INVESTIGATOR: Richard N. Zare

INSTITUTION: Stanford University
Office of Sponsored Research
651 Serra Street
Stanford, CA 94305-4125

1. Introduction

Mass spectrometry (MS) is a powerful analytical tool for determining the structural and chemical identities of a broad array of analytes that can be converted to gas-phase ions. MS possesses the advantages of rapid data acquisition, sensitivity, large dynamic range, and selectivity. Though different instruments employ different specific measurement principles, all mass spectrometers share the common goal of measuring parameters that can be converted to a histogram of mass-to-charge ratios. This goal is achieved through the manipulation and monitoring of ions exposed to known electric and/or magnetic fields. Unlike many other analytical techniques, mass spectrometry is completely general: any chemical species that can be made into a stable gas-phase ion can be analyzed. Ion source technologies, methods to produce gas-phase ions, have advanced rapidly. These new methods enable gas-phase ion generation from most types of chemical samples from both the solution-phase and the solid-phase without the need for any labeling or chemical derivatization.

Time-of-flight mass spectrometry (TOFMS) is perhaps the simplest and most cost-effective form of molecular weight analysis. In traditional TOFMS, an ion packet, a group of ions initially defined in time and space, is accelerated to a known, high kinetic energy and pulsed into a field-free drift region. Within this field-free region, the ion packet separates into its components based upon the different velocities of ions having different mass-to-charge ratios. A measurement of an ion's flight time from the initial gating pulse until the time of arrival at the detector determines the ion's mass-to-charge ratio, with proper calibration.

TOFMS is a pulsed analysis technique: it relies on the introduction of ion packets into the drift region, one packet at a time. The highest mass-to-charge ratio ion, and therefore the slowest moving ion, must arrive at the detector before a new packet is pulsed into the drift region. The time between pulses determines the mass range of the experiment. For pulsed ionization techniques including laser-based methods such as MALDI(Tanaka, Waki et al. 1988), SELDI(Hutchens and Yip 1993), and μL^2MS(Spencer, Hammond et al. 2008), the pulsed detection of TOFMS does not represent a limitation. Instead, for these methods pulsed detection is a clear advantage. However, for ionization methods that produce a continuous stream of analyte ions, such as electrospray ionization (ESI)(Fenn and Mann 1989), TOFMS is inherently inefficient because a large percentage of the ions generated, those formed between ion packet

pulses, are discarded. The figure of merit that describes the fraction of an ion beam sampled by a detector is called the duty-cycle. In the TOFMS analysis of a continuous ion source, mass range and duty-cycle are inversely coupled figures of merit.

Two main strategies are used to increase the duty-cycle of TOFMS: ion storage or orthogonal extraction. Ion storage uses an RF ion trap to store ions and selectively release accumulated packets into the TOF mass analyzer. This technique can allow TOFMS to approach 100% duty-cycle, but the simplicity and cost effectiveness of the technique are reduced, if not lost. Additionally, the dynamic information about beam evolution is averaged over the storage time, rendering this technique less suitable for measuring rapid kinetics. Another strategy for increasing the duty-cycle in TOFMS is to use orthogonal extraction. In this technique, the ion beam is pulsed into the drift region orthogonally from its direction of introduction into the mass spectrometer. With this strategy, duty-cycles of up to 1-10% can be achieved without expensive expansion of the apparatus. Very complex strategies involving multiple ion gates can increase it further at the cost of mass range.(Brenton, Krastev et al. 2007)

Our lab has developed an alternative solution to couple a continuous ion source to a TOFMS, one where duty-cycle and mass range are fully decoupled. Instead of introducing pulses of ions into a field-free region, we spatially modulate a continuous ion beam between two discrete states at megahertz rates according to a pseudorandom sequence. This spatial modulation takes the form of deflection of the ion beam off the axis of its initial propagation using a specialized device called a Bradbury-Nielsen gate (BNG).(Yoon, Zuleta et al. 2007; Zuleta, Barbula et al. 2007) The Bradbury-Nielsen gate is designed to allow short deflection rise-times and to confine the physical region within which the ions experience deflection. Because the pseudorandom sequences used to modulate the ion beam are based on Hadamard matrices, we call our technique Hadamard transform (HT) TOFMS. The key advantages of HT-TOFMS are:

1) Increased sensitivity and duty-cycle: By detecting the ions from both the deflected and undeflected channels, the technique achieves 100% duty-cycle. Because it counts more ions per unit time, HT-TOFMS is more sensitive than a traditional TOFMS.(Kimmel, Yoon et al. 2005)
2) Increased peak height precision: The high duty-cycle improves the precision of the peak heights per unit/time compared to traditional TOF experiments. This aids in

studying time-dependent processes where peak heights are used for absolute or relative quantitation.(Kimmel, Yoon et al. 2005)

3) Rapid spectral acquisition: Sensitivity increases can be traded for faster spectral acquisition rates. (Kimmel, Yoon et al. 2005)

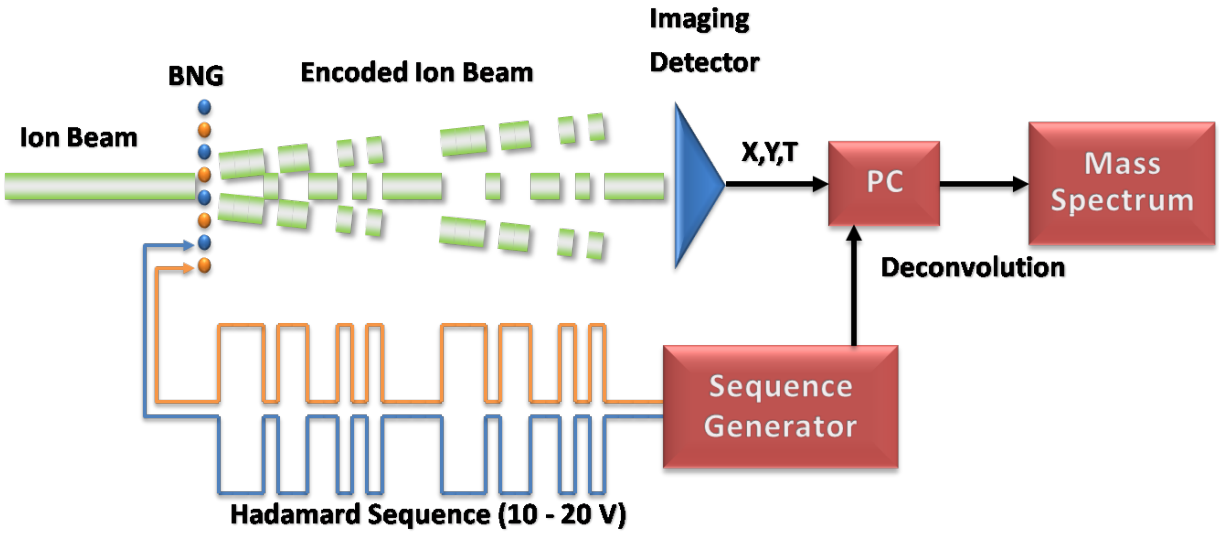

Figure 1: Schematic of the HT-TOFMS experiment.

The HT-TOFMS experiment is illustrated schematically in Figure 1. Two instruments have been constructed in our lab, one with a linear flight path (as shown in the figure) and one that employs a flight path with an ion mirror (not shown). In their current implementation, our HT-TOMFS instruments employ imaging detectors based upon MCP-coupled delay-line anodes. In this configuration, the MCP stack generates an electron cloud in response to an ion arrival event. The wires of the delay-line anode, differential pairs dedicated each to X and Y-position detection, collect the electrons from the emitted cloud. These collected electrons result in pulses of current that travel to the ends of the grounded wires. The arrival times of the two pulses at a detector placed at the end of each wire set encode the position and arrival time of an ion arrival event. From the data recorded at the detector, the flight time information can be decoded in a computer using knowledge of the sequence used to modulate the ion beam.

In addition to the ability to efficiently perform a 100% duty-cycle experiment, the data from the detector can be binned into pixels to image directly the ion beam profile as a function of mass-to-charge ratio. This capability provides the opportunity to produce the equivalent of a color movie of the ion beam, where the different ion arrival flight times correspond to colors in

the image. This new tool provides a method of studying chemical and physical processes that take place within the mass spectrometer.

2. Accomplishments

2.1 Optimization of the HT-TOFMS Experiment

The Hadamard sequences used in HT-TOFMS are composed of approximately half '1's and half '0's. Within this scheme the '1' element corresponds to ions that do not undergo deflection by the BNG and the '0' element corresponds to ions that undergo deflection. Thus, both the undeflected and deflected components of the ion beam contain approximately 50% of the ions of the initial beam. By measuring both the undeflected and the deflected beam components, a 100% duty-cycle measurement can be achieved be independent deconvolution of each group of ions and combination of the resultant spectra. Although a 100% duty-cycle measurement was theoretically possible in a configuration where two independent detector anodes where used for analysis of deflected and undeflected ions, this method posed substantial technical problems.(Kimmel 2004) In particular, this detection method required matching the beam position, size, and the deflection distance exactly to the detector anode dimensions. This requirement for matching the beam to the detector proved difficult to achieve in practice during the instrument development phase of AFOSR work, and, in all experiments, resulted in some reduction of the duty-cycle.

In the delay-line anode imaging HT-TOFMS scheme implemented here, a true 100% duty-cycle measurement is achieved for every experiment. The process of data collection is illustrated schematically in Figure 2. Data is collected as an array of arrival times and positions and then post-processed to define the detector regions that correspond to the deflected and undeflected components of the ion beam. Regions corresponding to the deflected and undeflected components of the ion beam can be isolated from an image generated from the sum of all ions collected during the course of an experiment. Each of these regions can be processed to generate encoded arrival time histograms where individual time bins contain ion contributions from all mass-to-charge ratio species. More specifically, the raw data, RAW, collected by extracting the

arrival time histograms for a detector region is the convolution of the true time-of-flight spectrum, TOF, including noise components, with the a right circulant matrix representation of the Hadamard sequence, SIM:

$$\begin{bmatrix} R \\ A \\ W \end{bmatrix}_{Nx1} = \begin{bmatrix} S \\ I \\ M \end{bmatrix}_{NxN} \times \begin{bmatrix} T \\ O \\ F \end{bmatrix}_{Nx1} \quad (1)$$

The true time-of-flight spectrum can be recovered from the raw data by a decoding process that results from multiplication of the raw data with the inverse of the right circulant matrix representation of the Hadamard sequence.

$$\begin{bmatrix} T \\ O \\ F \end{bmatrix}_{Nx1} = \begin{bmatrix} S \\ I \\ M \end{bmatrix}^{-1}_{NxN} \times \begin{bmatrix} R \\ A \\ W \end{bmatrix}_{Nx1} \quad (2)$$

The undeflected ions produce a "positive" spectrum, where the peaks in the time-of-flight spectrum correspond to positive intensity values. The deflected ions, in contrast, produce a "negative" spectrum, composed of peaks of negative intensity. The sign associated to the intensity peaks is a function of the correlation of the ion signal with the '1' element in the Hadamard modulation sequence. The full 100% duty cycle spectrum is generated by subtracting the decoded spectra from the deflected components of the ion beam from the undeflected. The observed signal-to-noise ratio of the observed spectra can be maximized by choosing the best windows during the data processing, which removes correlated noise between them.

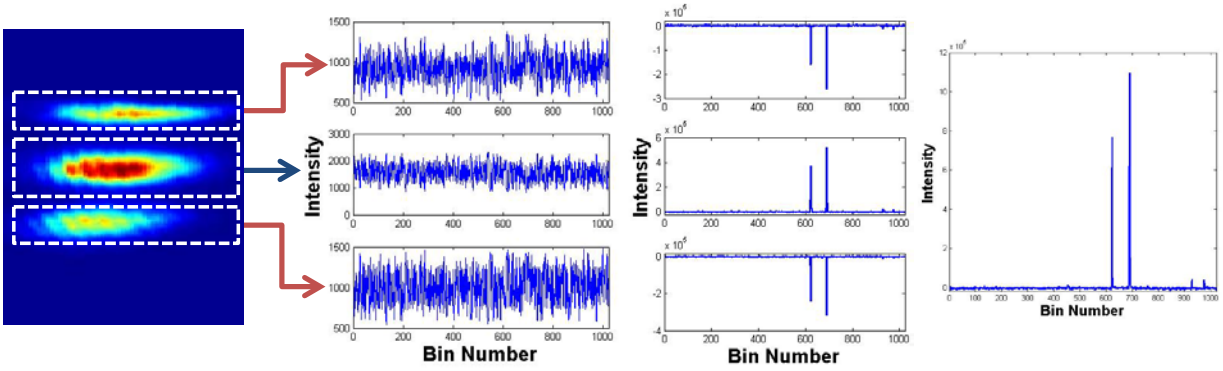

Figure 2: Schematic of the process of TOF data extraction from the ion arrival images generated in imaging HT-TOFMS.

The HT-TOFMS technique is a multiplexed analysis method, the arrival of ions of different mass-to-charge ratios occur within averaged time bins. Data on individual species must be extracted using mathematical manipulation. Multiplex measurement is ideal for systems

where the largest source of noise is independent of the magnitude of the signal. In these systems the maximum analytical advantage to multiplex analysis, the advantage in the relative variance when compared to one-at-a-time measurement, is a function of n, the number of objects that *must* be measured:

$$\frac{\sigma^2_{individual}}{\sigma^2_{multiplex}} = \frac{(n+1)^2}{4n} \approx \frac{n}{4} \qquad (3)$$

This advantage is significant, especially for systems where a large number of species must be measured. However, in electrospray mass spectrometry experiments, like HT-TOFMS, the dominant source of noise is the electrospray process itself. Electrospray ionization produces an ion beam which fluctuates on the timescale of the experiment and chemical noise that scales with signal intensity. The magnitude of fluctuation in electrospray current depends upon the intensity of the current. In most cases, the use of multiplexing in systems that exhibit signal dependant noise is disadvantageous: multiplexing actually results in a reduction of signal to noise ratio by a factor of $\sqrt{2}$ when compared to a scanning instrument. However, for sparse spectra like those we expect to collect using ESI-MS, which produces predominantly molecular ions, part of the original multiplex advantage can be retained. Our lab has worked to expand the theory of HT-TOFMS and mathematically prove the analytical advantage of the method.(Kimmel, Yoon et al. 2005)

For ion counting experiments, a better figure of merit for comparison, rather than signal-to-noise ratio (SNR), is peak height precision (PHP). SNR is mathematically related to the relative decrease in variance described in Equation 3. PHP is an alternative figure of merit that is defined as the peak height divided by its own standard deviation over many experiments. Within an ion counting scheme, the use of thresholding and signal intensity discrimination can artificially create background-free experiments which misrepresent SNR phenomena. For MS experiments that employ ion counting techniques SNR does not have the same interpretation as it does in optical spectroscopy. Because of the structure of the HT-TOFMS experiment, it employs ion counting but exhibits baseline noise that cannot be eliminated by thresholding the raw data. Thus, PHP is a better figure of merit for comparison of TOFMS with HT-TOFMS. In general, high PHP is important when the peak height is used for quantitation in experiments such as solution kinetics or coupling with chromatography techniques. In the shot-noise limit, the multiplexing advantage in peak height precision is given by(Kimmel, Yoon et al. 2005):

$$\frac{\mathrm{PHP}_i^{\mathrm{HT}}}{\mathrm{PHP}_i^{\mathrm{Conv}}} = \sqrt{\frac{f^{\mathrm{HT}}}{f^{\mathrm{Conv}}} F_i} = \sqrt{N F_i} \qquad (4)$$

Here, $\mathrm{PHP}_i^{\mathrm{HT}}$ and $\mathrm{PHP}_i^{\mathrm{Conv}}$ are PHPs of analyte *i* in 100% duty-cycle HT-TOFMS and conventional TOFMS modes. F_i is the fractional abundance of a particular species *i* in the ion beam analyzed. N is the length of the Hadamard sequence used in the measurement. This equation can be used to consider the suitability of a HT-TOFMS experiment in place of any other MS measurement whose duty-cycle is known. As long as the fractional abundance of the ion species exceeds the duty-cycle ratio, HT-TOFMS will provide a PHP advantage versus the same experiment analyzed using traditional TOFMS. To provide a numerical example, for a 2047 element sequence, any peak that contains more than 1/2047$^{\mathrm{th}}$ of the ion current, or approximately .05%, will be detected with enhanced peak height precision over conventional TOFMS.

This limitation in the capability of HT-TOFMS is not immediately obvious and can be understood by realizing that multiplex methods detect more species per unit time, but, as a consequence, they smear out the noise from each measurement evenly across all species measured. For systems with signal-independent noise, the net effect of multiplexing is to simply make and average the result of more measurements. However, for systems with signal-dependent noise, the net effect is to produce an averaged signal that subjects the less intense peaks to the increased noise associated with measuring the more intense peaks. This increase in noise can ultimately make it impossible to distinguish peaks from the background that could have otherwise been distinguished with a dispersive method and a longer observation time.

To illustrate the experimental PHP advantage of HT-TOFMS over traditional, on-axis TOFMS, the mass spectra of a mixture of rhodamine 6G (479 amu) and reserpine (609 amu) has been analyzed at various acquisition times in both measurement modes. The results are shown in Figure 3 and summarized as a table in Figure 4. The mass spectra were taken for acquisition times of 1 s (Figure 3 A and B), 100 ms (Figure 3 C and D), and 10 ms (Figure 3 E and F). The experiments were repeated 16 times to obtain the error bar in the peak heights. The standard deviations of the peak heights are shown as vertical error bars. Panels A and B compare the two techniques for an acquisition time of 1 s. As shown by the smaller error bars, the peak heights are more stable in the Hadamard mode compared to the conventional mode at all acquisition times. For the 1 s acquisition, Hadamard mode PHPs are 41 and 23 for rhodamine 6G and reserpine, respectively. Conventional mode PHPs are 4 and 3 for rhodamine 6G and reserpine for the same

acquisition time. For rhodamine 6G, this comparison represents an improvement of about 10 times in PHP, which is smaller than the theoretical improvement of $\sqrt{2047 \times 0.25} = 23$ under shot noise limited conditions. The value of 0.25 under the radical reflects the approximate fraction of the total ion current that is present in the peak bin for both rhodamine and reserpine. Each species was assumed to contribute half of the ion current and that the bin of maximum intensity corresponds to one half of the total ion current in the peak. The deviation from the theoretical improvement value is mainly due to fluctuations in the electrospray current, which is not taken into account in the theoretical derivation, and the effects of imperfect beam modulation.

In both panels A and B of Figure 3, the same qualitative conclusions can be made from the mass spectra collected using traditional TOFMS and HT-TOFMS. However, as the acquisition time is reduced such that the effects of ion statistics become dominant, the PHP improvement corresponds to an enhancement in the analytical value of the spectra, as shown in panels C and D of Figure 3 for an acquisition time of 100 ms. For the conventional mode, there are not enough ions to consistently observe a mass spectrum, however some individual 100 ms spectra show distinct peaks. In contrast, in the Hadamard mode, the peaks are well discriminated from the baseline and the peak heights are still very stable. In this case the PHPs of rhodamine 6G and reserpine are 15 and 18 for Hadamard mode and 1.1 and 1.7 for conventional mode. This improvement in PHP of 14 and 11 is still less than the shot noise limiting theoretical value of 23. This effect is even more pronounced (see Figure 3 E and F) at even shorter acquisition times (10 ms). In these panels the PHPs of rhodamine 6G and reserpine are 11 and 5.7 for the Hadamard mode and 0.6 and 0.4 for the conventional mode, representing improvements of 18 and 14, respectively. This improvement in PHP at short acquisition times is particularly useful, as will be shown later, in the quantitative analysis of peak heights that vary with time.

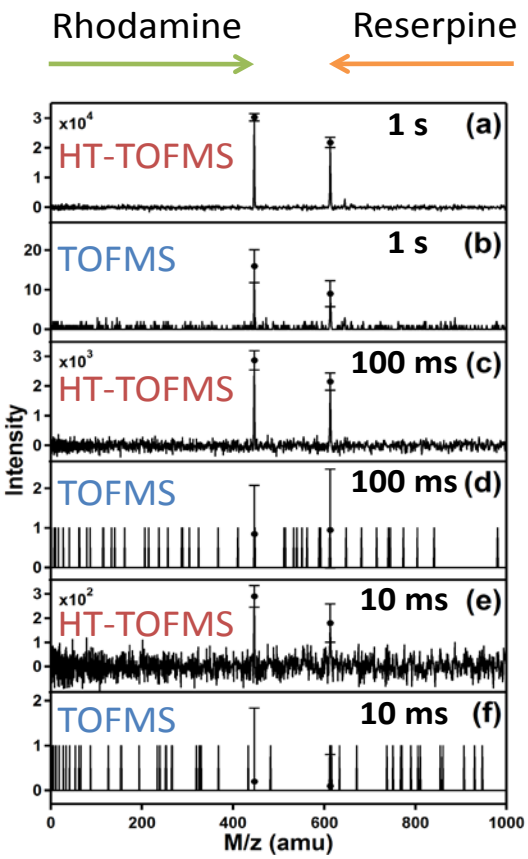

Figure 3: Peak height precision enhancement study of a mixture of rhodamine 6G (479 amu) and reserpine (609 amu) showing the spectral acquisition (a) of 1 s in Hadamard mode; (b) of 1 s in conventional mode; (c) of 100 ms in Hadamard mode; (d) of 100 ms in conventional mode; (e) of 10 ms in Hadamard mode; and (f) of 10 ms in conventional mode. The error bars are calculated from 16 experiments. Each plot is for one representative spectrum and dots represent the average peak heights.

Acquisition Time	PHP Gain HT-TOF vs.TOF	
	Rhodamine	Reserpine
1 s	10	8
100 ms	14	11
10 ms	18	14
Theoretical	23	18

Figure 4: PHP gain from HT-TOFMS over traditional TOFMS from the experiments detailed in Figure 3.

2.2 Studies Exploiting Imaging Capabilities

When implemented using an imaging detector, HT-TOFMS has the capability to provide a mass spectrum for every pixel of a two-dimensional detector surface. In this method, which requires a collection of a significantly larger number of ions than a typical HT-TOFMS experiment, each pixel is separately deconvoluted, rather than being deconvoluted as part of a defined deflection state group. A series of such images correspond to a mass-to-charge resolved movie of the ion beam within the instrument. Ions that undergo chemical or physical processes that occur within the instrument will appear at different positions at the detector due to the spatial effects of the process or the result of interaction with the electric fields within the instrument. Analysis of the differences in arrival position can be used to extract extra chemical information beyond and in addition to the mass-to-charge ratio of a chemical species. As a demonstration of the capability of the imaging HT-TOFMS to spatially and temporally resolve chemical processes, we have investigated ions fragmented by surface-induced dissociation (SID) inside the reflectron and ions that fragmented spontaneously through post-source decay (PSD). In this work we show the physical separation and separate analysis of precursor and fragment ions in HT-TOFMS.

PSD is a form of unimolecular decomposition that occurs on the microsecond time scale for ions that possess high, but not extreme, total internal energy, and is a common feature of MALDI mass spectra for instruments that employ a reflectron.(Kaufmann, Kirsch et al. 1994) Because PSD fragment ions maintain the velocity of their precursors, they contribute only to the precursor ion intensity in TOFMS instruments with a linear geometry. PSD ions can be treated as subtype of the metastable ions that were studied in detail in the 1960's and 1970's using double focusing sector mass spectrometers.(Cooks, Beynon et al. 1973) These ions are characterized by having sufficient stability to leave the ion source region intact, but being sufficiently unstable in that they fragment within the instrument before reaching the detector.

SID(Dongré, Somogyi et al. 1996) is a fragmentation technique in tandem mass spectrometry in which ions are forced to collide with a surface. Upon collision, some fraction of an ion's incident kinetic energy is converted into internal energy. Often enough energy can be transferred so that the level of internal energy exceeds the bond dissociation energy of the ion's weakest bond and causes fragmentation. The process for collisional activation is similar to the

more common collision-induced dissociation (CID), however in SID the collision partner is a solid surface rather than another gas-phase atomic or molecular species. In the SID and CID analysis of protonated peptides, the protonated amide bond, the weakest bond in the molecule, is the most likely site of bond cleavage. The predominance of this fragmentation pathway indicates that there is some degree of energy reorganization before the fragmentation event occurs. Some advantages of SID over CID are greater energy transfer efficiency and better vacuum compatibility. In its most common implementation, the SID surface is mounted between two mass analyzers with non-linear geometry.(Schey, Cooks et al. 1987; Schey, Graham Cooks et al. 1989; Wysocki, Ding et al. 1992) Typically, this configuration is completed with an SID surface mounted between to quadrupoles, in a scheme similar to the triple quadrupole mass analyzer where the second quadrupole is used as a collision cell for CID. In an alternative configuration, one group has implemented SID in a quadrupole-TOFMS system where, during tandem MS experiments, the quadrupole analyzer serves as the initial mass selection stage and TOFMS is used to analyze the SID fragments.(Galhena, Dagan et al. 2008)

Several groups have performed SID in TOFMS using a surface placed inside a reflectron.(Williams, Jones et al. 1992; Williams, Fang et al. 1993; de Maaijer-Gielbert, Beijersbergen et al. 1996) The construction of in-reflectron SID TOFMS systems has been limited because the technique places substantial and inconvenient requirements on instrument geometries. Typically, two methods are used to construct in-reflectron SID-TOFMS systems. In one method, the backplate, the last electrode in the reflectron, typically located several (10's) centimeters from the entrance of the reflectron for normal operation, can be moved very close to the reflectron entrance for SID experiments. In this scheme the backplate must be a solid electrode, rather than a grid. In this geometry, ions are rapidly decelerated in the reflectron before collision with the surface and reaccelerated towards the detector only after their remaining velocity upon the reflecting/collision event allows them to translate away from the backplate. This design does not allow for efficient collection of fragmented ions. Placement of the reflectron backplate closer to the front of the reflectron is the method used to increase fragment collection efficiency. Alternatively, other groups have used an SID surface placed at a deeper reflectron backplate after a deceleration/extrication grid that is fixed in position. In this design the SID fragments had to be extracted from the near-surface area and pushed through the reflection using delayed extraction by pulsing the voltage applied to the grid.(Haney and

Riederer 1999; Gamage, Fernandez et al. 2004) This method using extraction pulses aids in efficient fragment collection, but increases the complexity of the electronic component of the instrument design.

For the present work, we studied SID using a modified two-stage reflectron with the SID surface mounted to a gold-plated stainless steel plate that was electrically connected to one of the reflectron electrodes, number thirteen, counting from the entrance to the reflectron, of twenty-one in total. This gold-plated steel plate could be horizontally translated in and out of the ion beam path with a linear manipulator (660008, MDC Vacuum Products, Hayward, CA). A self-assembled monolayer of 2-(perfluorodecyl)ethanethiol was formed on the gold-plated stainless steel plate before placing it in the vacuum system.

Self-assembled monolayers of fluorinated alkane thiol species have been shown to enhance the fragmentation yield in SID experiments and were prepared to enhance the probability of detecting this phenonmenona under the non-ideal conditions chosen for this experiment.(Morris, Riederer et al. 1992) In this scheme, the collision energy of the surface-induced dissociation can be varied by changing the reflectron voltage settings. The collision voltage is calculated as the difference between the acceleration voltage and the voltage on the SID electrode. The collision energy can be calculated by the sum of the initial kinetic energy before acceleration and the collision voltage multiplied by the charge of the precursor ion. In this work we will assume that initial kinetic energy of the ions makes a negligible contribution to the collision energy of the ions.

$$E_{collision} = z \cdot e \cdot V_{collision} + E_{initial} \qquad (5)$$

Equation 5 can be used to calculate the collision energy of an ion with a surface, where z is the charge number of the ion, e is the charge on an electron, $V_{collision}$ is the collision voltage, and $E_{initial}$ is the initial, preacceleration, kinetic energy of the ion. For example, a collision voltage of 30 V for our triply charged precursor should correspond to collision energy of 90 eV. In a typical SID experiment, 5-30% of the collision energy can be converted to internal energy upon collision.(Dongré, Somogyi et al. 1996)

A schematic of our reflectron design in which the manipulator and SID surface are within the reflectron is presented in Figure 5c, where the manipulator is out of the path of the ion beam. In Figure 5d the apparatus is shown with the surface in the path of the ion beam.

Triply charged angiotensin I (10 μM, American Peptide, Inc., Sunnyvale, CA) was used for all experiments and electrosprayed in a solution of 50:50 v/v of methanol (Sigma Aldrich) and water (18 MΩ, Millipore, Billerica, MA). Most tandem MS techniques require precursor ion selection. By controlling the electrospray solution conditions and the ion source settings, we were able to generate an ion beam that when analyzed by MS showed only the triply charged angiotensin I peak. In this manner the need for precursor selection is avoided. However, to use HT-TOFMS combined with SID for future ion fragmentation or tandem mass spectrometry experiments, it will be necessary to use a stage for mass selection or limit analysis to systems that have a single peak in their precursor mass spectrum.

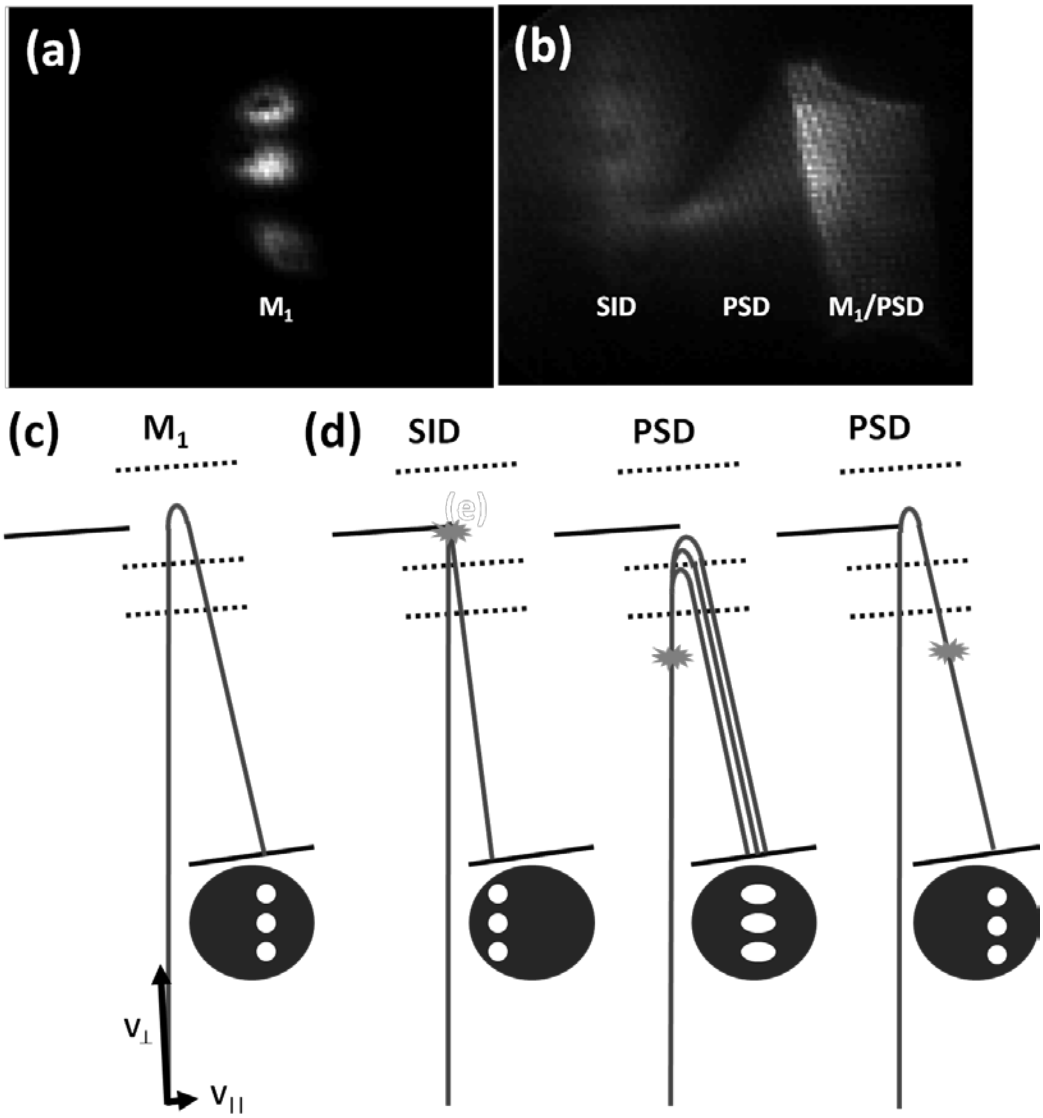

Figure 5: Schematic of the experiment. Two-dimensional images of triply charged angiotensin I (433 amu) with the SID surface (a) withdrawn and (b) inside the reflectron. Illustrations showing the trajectories and arrival patterns at the detector of (c) precursor ions and (d) three fragmentation processes: SID, PSD pre-reflectron, and PSD post-reflectron. PSD does occur inside the reflectron but is spread in position and time between pre- and post-reflectron PSD signals.

Figure 5a and Figure 5b present the 2D images of *x*, *y* positions of the ion beam when the ion beam path is clear and blocked by the SID surface corresponding to the schematic diagrams in panels c and d, respectively. Figure 5a shows regions of ion intensity that correspond to the deflected and undeflected components of the precursor ion beam. Comparison of the images of Figure 5 reveals a more detailed image of the beam structure and what happens when that beam is forced to interact with an SID surface. The image with the ion beam partially blocked by the SID surface, Figure 5b, shows that the normally well-defined ion beam has blurred and new regions of ion intensity appear across the detector. For reasons that will be discussed later, we attribute the new regions of ion intensity to different fragmentation processes, SID and PSD, which have been spatially separated within the reflectron. With the SID surface in the fragmentation position, some of the precursor ions will pass by the surface and reach the detector without interacting with it; these non-interacting precursor ions are labeled M_1. These different processes are explained schematically in Figure 5d. It is important to note that blocking the ion beam with the surface results in a substantial reduction in the recorded ion intensity. The ion arrival rate in Figure 5b, which is a sum over several minutes, is approximately 2% of the rate recorded in Figure 5a. Thus, the data collected in Figure 5b took several hours. Figure 5c and Figure 5d include a cartoon highlighting the expected spatial separation of fragmented and unfragmented ions. If an ion does not fragment, Figure 5c, or if it fragments after exiting the reflectron, Figure 5d, it will reach the detector at high *x* position, farther to the right. If an ion fragments before or inside the reflectron, its flight time will be reduced and the fragments will arrive at the detector at a smaller *x* position, toward the left (Figure 5c).

Spatial separation of the different fragmentation processes along *x*-axis happens inside the reflectron because the reflectron is horizontally rotated by 4 degrees relative to the initial ion beam propagation direction. The ions that undergo SID will be reflected based upon the relative position and angle of the SID surface. The separation of pre-reflectron PSD ions has a specific mathematical relationship and can be better understood by considering the vector components of a precursor ion's velocity. The velocity of a precursor ion at the entrance to the reflectron can be divided into two components that are parallel ($v_{\parallel}$) and perpendicular ($v_{\perp}$) to the reflectron electrodes. A reference to the physical definition of parallel and perpendicular with respect to the reflectron is shown in the bottom left-hand corner of Figure 5c. The *x* position of ion arrival at the detector is given by the product of the parallel velocity component and the flight time

because the parallel velocity component does not change upon fragmentation or deceleration/acceleration in the reflectron (except slight modification from kinetic energy released).(Cooks, Beynon et al. 1973; Laskin and Lifshitz 2001) The perpendicular velocity component will change during deceleration and reacceleration in the reflectron. The recorded flight time will change depending on the position of the fragmentation event and the mass and charge of the fragment. This specific relation between x-position and arrival time will allow the characterization of the PSD process independently from more common phenonmenona.

The flight time of a PSD-fragmented ion is typically reduced because its kinetic energy is divided between the two fragment ions according to the ratio of their masses. This scheme is described in Equation 6 where precursor ion M_1^{+x}, of mass M_1 and charge x breaks into two fragments, M_2^{+y} and M_3^{+z} with corresponding mass M_2 and M_3 and charges y and z. The value of either y or z may be zero within this scheme, but their sum must be conserved.

$$M_1^{+x} \rightarrow M_2^{+y} + M_3^{+z}\colon\ x = y + z \tag{6}$$

The kinetic energy of M_2^{+y} is given by Equation 7:

$$KE(M_2^{+y}) = \frac{M_2^{+y}}{M_1^{+x}} KE(M_1^{+x}) = \frac{M_2^{+y}}{M_1^{+x}} xeV_0 \tag{7}$$

where e is the charge on an electron and V_0 is the initial acceleration voltage. The velocities of the fragments will be the same as the precursor ion, M_1^{+x}, however the kinetic energies of the fragments will partition according to the relative masses of the fragments. Thus, common fragment ions are reflected by the reflectron at an earlier stage (lower potential) due to reduced kinetic energy per unit charge. For fragmentation of multiply charged ions where the fragment ion has a large mass and a different charge from the precursor ion, the kinetic energy per unit charge will be greater. In this case, the PSD fragment will arrive at the detector after the flight time expected for its precursor.

Thus, for PSD fragments, the position, *x*, and the flight time *t* will be highly correlated with a slope given by the parallel velocity component. The *x* position will deviate from this correlation if an ion collides with the SID surface because it will lose most of its kinetic energy upon collision. Its new velocity will be determined by the interaction with the surface. Then, it will be reaccelerated in a direction perpendicular to the surface reaching the detector at a lower *x* position (Figure 5d). Therefore, SID and PSD fragment ions will have very different correlations between *x* and *t*, which allows us to study these two processes separately.

The 3D histogram (*x*, *y*, *t*) for a SID collision voltage of 12 V (36 eV collision energy) (Figure 6a) was deconvoluted with a Hadamard sequence along the time axis, to produce time-of flight resolved images of the ion beam at the detector. The image cross-sections at various flight times are shown in Figure 6b through Figure 6f, where positive and negative intensities are displayed as red and blue, respectively. Recall that a negative intensity represents a negative cross correlation with the Hadamard sequence and corresponds to the detection of ions deflected according to the Hadamard sequence. Characteristic Hadamard deflection patterns of negative-positive-negative beams are seen at different positions in the images with quite different flight times. Figure 6a is the 2D image of the ion counts, the same as shown in Figure 6b, for comparison.

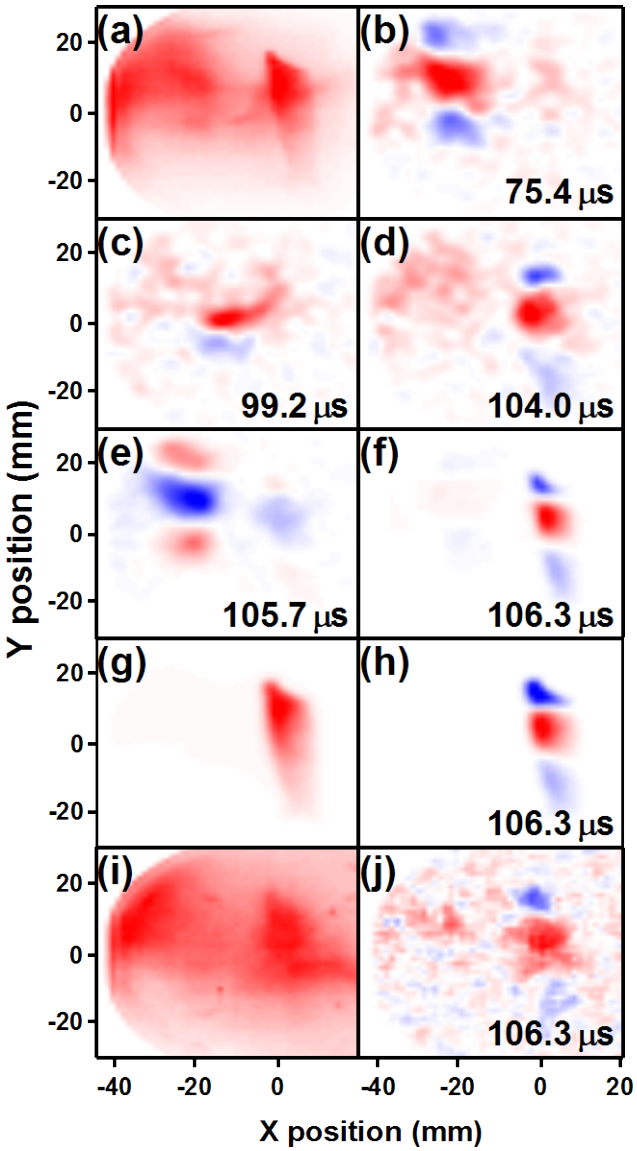

Figure 6: Spatially resolved TOF images angiotensin I undergoing SID at collision energy of 90 eV. a) *xy* image of total ion counts summed over time and (b−f) *xy* images at different flight times at a detector grid at 0 V. SID is apparent in parts b and e, PSD is apparent in parts c and d, and the precursor ion appears in part f. The detector grid is at 1500 V in parts g and h and 2000 V in parts i and j where parts g and i are the ion counts summed over time, and parts h and j are images at flight times that show only the precursor ions.

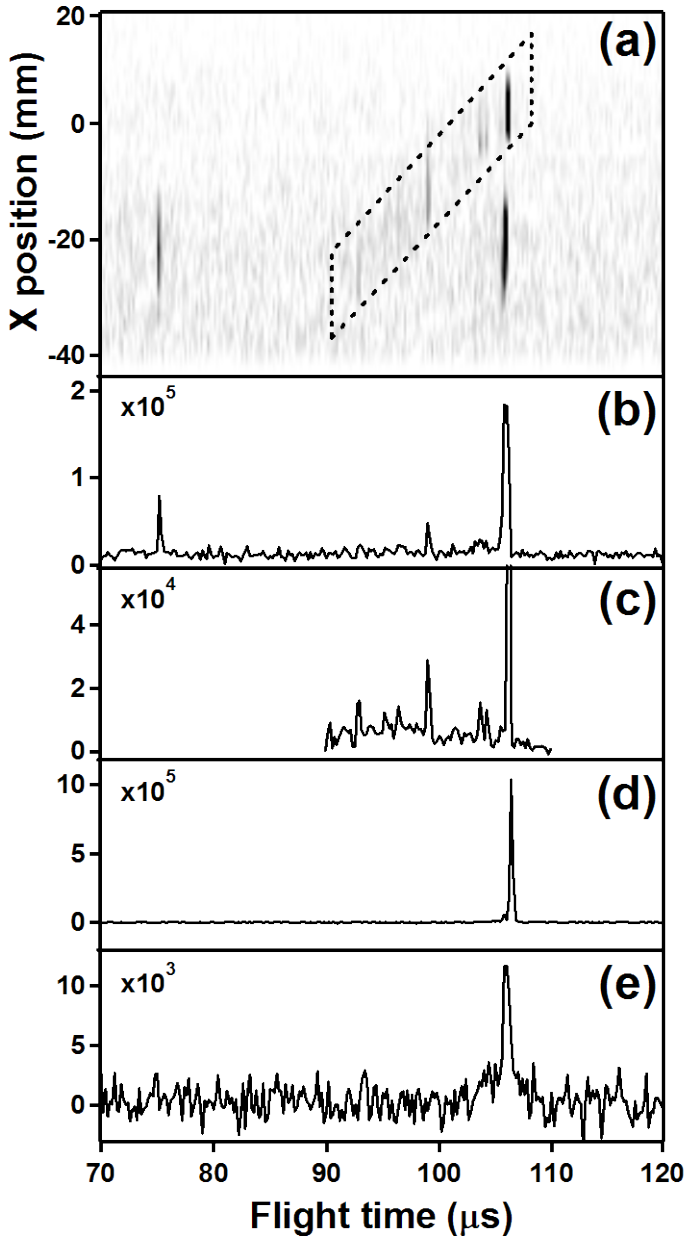

Figure 7: Mass spectra for data presented in Figure 6. (a) 2D plot of *x* position and flight time with the detector grid at 0 V in which the PSD fragment ions lie within the dotted box and (b−e) flight time spectra obtained (b) by summing over *x* positions, (c) by summing the dotted box region over *x* positions, (d) with detector grid at 1500 V, and (e) with detector grid at 2000 V.

A 2D plot of *x* position and flight time is shown in Figure 7a. The PSD fragments lie inside the dotted box, where the *x* position and flight time have a linear correlation with a slope of 1800 m/s. This velocity is the expected parallel velocity component of triply charged angiotensin I, which is calculated from an acceleration voltage of 1500 V and a 4 degree rotation of the reflectron. The most intense peak inside the dotted box at 106.3 μs is from the precursor ions. There are two other intense peaks outside the box at an *x* position of -21 mm and flight times of 75.4 and 105.7 μs. The *x* position is the same for the two peaks suggesting that most of the kinetic energy of the ions has been lost upon collision with the SID surface. The *xy* images of the two SID fragments (Figure 7e) are moderately broader than that of the precursor ions at 106.3 μs (Figure 7f). We attribute this behavior to the angular distribution of the ions off the surface. The flight time spectrum obtained by summing over *x* positions (Figure 7b) would be the mass spectrum expected from an SID experiment using a TOFMS without an imaging detector. Note that most of the PSD fragments are hidden in the baseline and also the precursor ion at 106.3 μs and the SID fragment at 105.7 μs are shown as a single peak. The peaks inside the dotted box were summed over *x* position, and the flight time spectrum is shown in Figure 7c, which is the spectrum of PSD fragments that are normally not visible in electrospray mass spectrometers. We are able to observe them because they have been separated from other intense peaks. To our knowledge, this work represents the first observation of PSD in electrospray ionization mass spectrometry. The peaks at 75.4 and 105.7 microseconds are tentatively assigned to the histidine immonium ion at 110 amu and double charged angiotensin I at 649 amu. Immonium ions are internal fragments that result from a combination of a-type and y-type* fragmentations and contain only a single side chain.(Falick, Hines et al. 1993) Immonium ions have the general chemical formula of $RCH{=}N^{+}H_2$ and are common diagnostics for the presence of a particular amino acid in the sequence of a polypeptide sample. Histidine forms immonium ions with high probability compared to other amino acids, and the probability of forming immonium ions of all types increases with collision energy.(Ioannis 1995) The commercial

*The designation of a-type and y-type fragmentation follows the standard nomenclature proposed by Roepstorff. (Roepstorff, P. and J. Fohlman (1984). "Letter to the editors." Biological Mass Spectrometry **11**(11): 601, Paizs, B. and S. Suhai (2005). "Fragmentation pathways of protonated peptides." Mass Spectrometry Reviews **24**(4): 508-548.) Within this scheme peptide backbone fragmentation is signified by a single letter. A, B, and C are used to describe fragments where charge is retained by the N-terminal fragment and X, Y, and Z are used to describe fragements where charge is retained by the C-terminal fragment. Thus, A-X ions correspond to the C-C bond breaking, B-Y ions correspond to C-N cleavage at the carbonyl carbon, and Z-C ions signify N-C bonds breaking at the side chain-containing carbon.

spectrum (not shown) matches the SID spectrum in that the immonium ion is the most prominent peak.

To confirm that the ions centered at 0 mm are uncollided ions and the ions at small *x* position, less than -20 mm, are fragmented ions, we repeated the experiment with the voltage on the grid in front of the detector at 1500 V relative to the flight chamber, which is the same voltage used for acceleration of the ions. The SID surface is at a potential lower than 1500 V so ions that undergo SID will have energies per unit charge less than 1500 V and will not appear at the detector. As noted above, some ions that undergo PSD may have more kinetic energy per unit charge and arrive at the detector under these conditions. The assignment of ions that arrive on the left of the detector to SID fragments is clearly shown in Figure 7g, where all the ions at smaller *x* positions have been removed. After Hadamard deconvolution, the time-of-flight spectrum shows a single peak at 106.3 μs (Figure 7d). The *xy* image at this flight time is in Figure 6h, which is identical to the image at the same flight time when the grid voltage was zero (Figure 6f). We assign this image to the precursor ions.

We also repeated the experiments with the grid in front of the detector at 2000 V, which is higher than the reflectron backplate voltage of 1900 V. Because the grid is set to a voltage above the back plate of the reflectron, ions that have enough kinetic energy to pass the grid will not be reflected by the reflectron. At this setting, all ions reflected by the reflectron will be blocked and only neutral molecules will be detected (Figure 6i). Closer inspection of Figure 6i reveals a broad smear at small *x* positions, which comes from neutrals generated by SID, and a broad smear at high *x* positions, which comes from neutrals generated by PSD. The neutrals generated by SID will not be accelerated by the reflectron and will have a small velocity. Also, the neutrals generated by PSD inside the reflectron will have a small velocity with a continuous distribution depending on the position of the fragmentation. Thus, for these neutrals, the Hadamard modulation will be blurred out in time. If PSD happens before the reflectron, the neutral molecules will be travelling away from the detector and will not reach the detector. If PSD happens after exiting the reflectron, the velocity will not change and the neutral molecules will maintain the timing from Hadamard modulation, (Figure 6e). The *xy* image at this flight time also has the Hadamard modulated ions at high *x* position (Figure 6j), which shows that PSD is happening after the reflectron. The same study was repeated at a higher collision voltage (80 V) and the results are similar to what is presented in Figure 7, but show more SID peaks.

One requirement for Hadamard imaging is that the Hadamard modulation must be maintained during the fragmentation processes. The neutral molecules that are created at collision with the surface will not be accelerated by the reflectron and will lose the timing information. Some of these molecules will reach the detector, but will only contribute to the background noise. The modulation efficiency for the SID processes is low at about 25% compared to 90% for precursor beam. This loss in modulation efficiency is mainly from the presence of neutral molecules. Because the 5 MHz Hadamard modulation (200 ns time bin) is maintained during SID and there is no tailing of the SID peaks, these images suggest that the surface-induced dissociation happens within about 200 ns. This conclusion is consistent with the results from the SID kinetics experiment by Gamage *et al*.(Gamage, Fernandez et al. 2004) Presently, the spatial resolution of the imaging HT-TOFMS is about 100 μm, but the images are much poorer, which is caused by the size of the ion beam. Future improvements in ion beam collimation optics at the ion source should markedly increase the image resolution. Nevertheless, the present resolution in space and time is sufficient to allow us to observe SID and PSD processes.

2.3 Characterization of DESI using HT-TOFMS

In another study, we have expanded the characterization of desorption electrospray ionization (DESI) through exploring rapid sampling rates and probing the rise and fall times of ion signals. These experiments were completed using a specialized DESI ion source coupled to HT-TOFMS. The continuous counting of ions in HT-TOFMS allows it to be efficiently coupled to continuous ion sources like DESI without requiring a trapping stage. This efficient coupling enables mass spectral measurement with a high temporal resolution for events occurring outside the mass spectrometer. This unique advantage of HT-TOFMS has aided in the collection of data that offers unique insight on the features and analytical limitations of the DESI mechanism. In the following experiments, we utilize a disk spotted with analytes which was spun at varying speeds to expose analyte-covered regions of the disk to the DESI plume for short, controlled residence times, down to tens of milliseconds, giving a programmable sampling frequency. Additive combination of data from multiple passes of the disk is used to probe the rising and

falling edges of the analyte signal. An upper bound for the maximum possible temporal resolution and sampling rate of DESI in the absence of sensitivity constraints is estimated and found to exceed previous DESI sampling rates.

Figure 8 shows a diagram of the DESI apparatus for the analysis of patterned disks. Disks were designed and machined out of poly(methyl methacrylate) (PMMA) with dimensions matching miniature compact disks, 8 cm in diameter with a 1.48 cm hole in the center. Red and blue Sharpie markers (Sanford Corporation, Oak Brook, IL) were used to draw the imaged pattern and sample spots. The detected components of the red and blue markers were rhodamine 6G and basic blue 7, respectively.(Ifa, Wiseman et al. 2007) The patterns were drawn by hand with the aid of a ruler and were imaged on the same day. A stepper motor with an integrated controller (23MD, Anaheim Automation, Anaheim, CA) was used to rotate the disk. The motor was driven by TTL pulses from a DS345 function generator (SRS, Sunnyvale, CA). The stepper motor was operated at 1600 steps per revolution producing nearly continuous rotation on the time scale of most experiments. The apparatus was capable of controlling speeds of rotation up to 20 Hz. The disks and stepper motor were interfaced using a mount made of anodized aluminum that held the disks through their center holes. The DESI source was constructed from the electrospray head of a ThermoFinnigan LTQ (San Jose, CA) ESI source. With the use of a custom-made mount, the head was interfaced to an *x*, *y*, *z* manipulator and a ball and socket pivot joint, allowing for easy linear and rotational translation. The stepper motor holding the disk was mounted on a separate *x*, *y*, *z* manipulator. The emitter was held at a potential of +5 kV. Dry nitrogen (Praxair, Danbury, CT) was used as a nebulizing gas. The spray solvent was a mixture of water and methanol (1:1 v/v) with 0.1.0% glacial acetic acid (Sigma -Aldrich, St. Louis, MO). Spectra were collected with flow rates ranging from 5-50 µL/min controlled via a syringe pump (Harvard Apparatus, Holliston, MA).

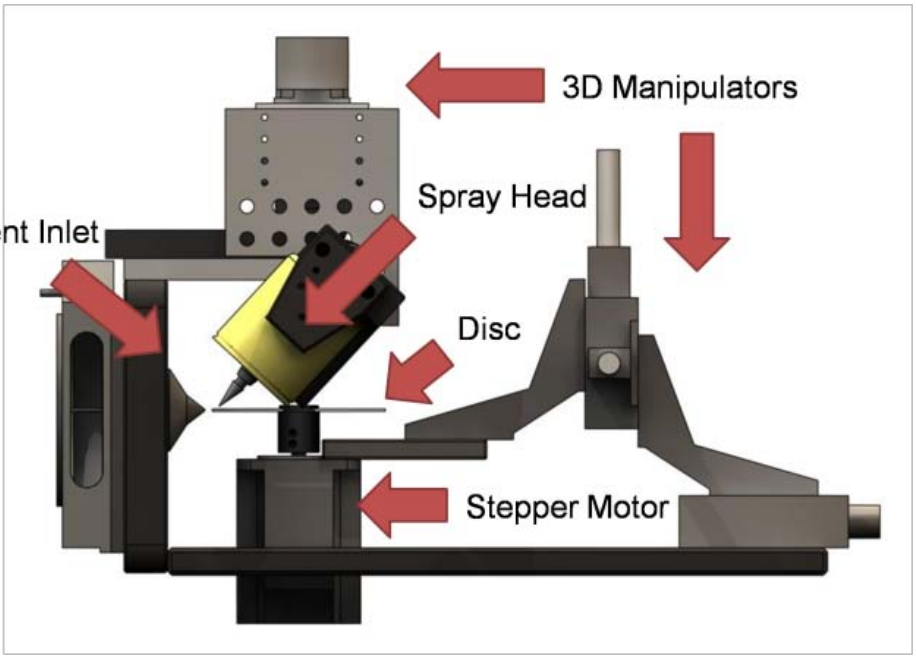

Figure 8: Disk platform for rapid DESI analysis.

One potential application of DESI with great promise is online or process monitoring. Chen et al. have suggested the evaluation of pharmaceutical products using pill-by-pill analysis on a moving assembly line.(Chen, Talaty et al. 2005) We have used our system to evaluate the fundamental limits of such a protocol where each analyte undergoes a single pass through the analysis window. By patterning a disk with alternating blank and chemically labeled regions, a pill-by-pill system can be modeled as shown in Figure 9b. Pills are three-dimensional objects and thus are less ideal surfaces for a DESI experiments. In our pill-model we divided the disk into eight sectors, where each sector was approximately 3.1 cm in length at the edge where the disk was analyzed. Sample spots were drawn using a marker containing basic blue 7. The stepper motor was programmed to produce rotation rates equivalent to different numbers of sample spots per second. Figure 9a shows the ion intensity from the basic blue 7 peak taken from a series of spectra collected at varying rates of rotation. The 0.5 s time window shown corresponds to multiple rotations of the disk. The HT-TOFMS data collection scheme allows the determination of the spectral acquisition rate after the analysis has been completed and can be matched to provide appropriate time resolution for different sample rates. The data presented in Figure 9a is shown at 200 spectra/s. The rate of 200 spectra/s is limited by the average ion count rate collected by our HT-TOFMS. For a typical count rate of 100 000 ions/s, the 200 spectra/s rate corresponds to spectra representing 500 ion arrival events within the 5 ms time bin. The use of

the 5 ms time bins allows for analysis at rates up to 80 samples/s by defining a peak by using two to three points. Defining a peak using one point is difficult because the spectral averaging time and residence time of the analyte would need to be synchronized to see ion signals return to a baseline value, making every measurement a changing average value of analyte and blank disk. The use of two to three points is insufficient to provide a chemical image of the surface and peak height stability but allows for determination of presence or absence because some fraction of the peaks are solely analyte.

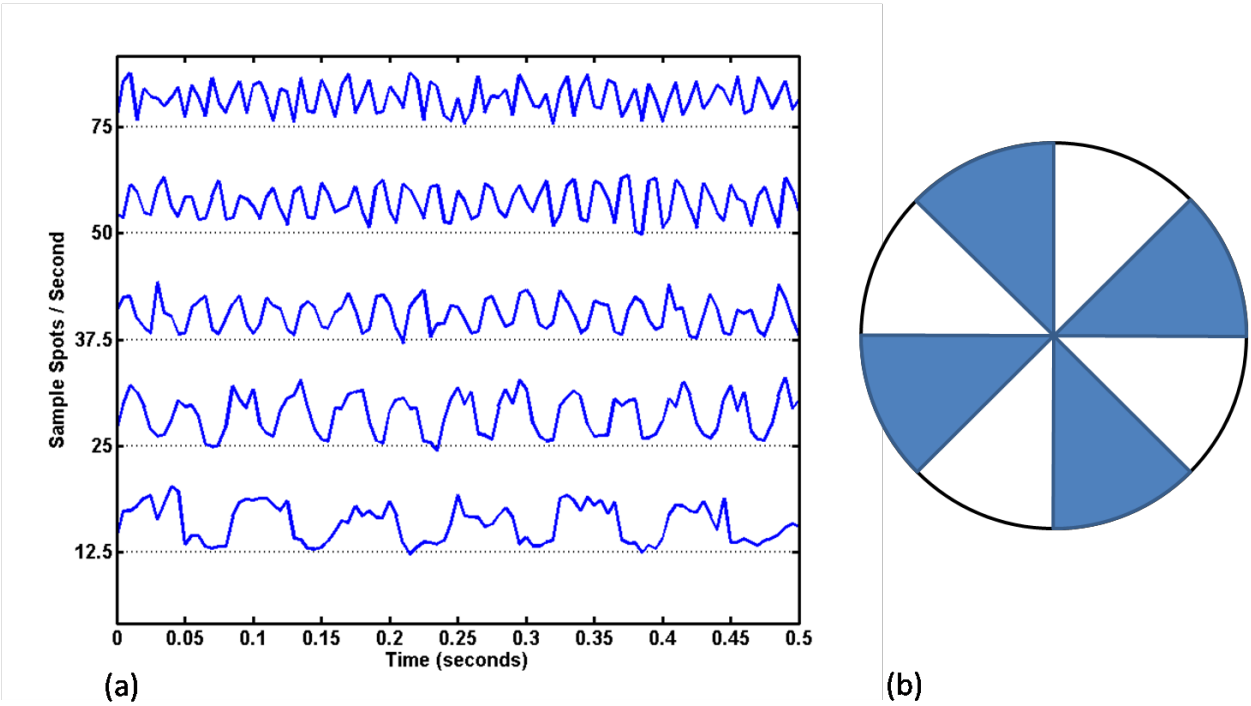

Figure 9: (a) Ion intensity of the basic blue 7 peak plotted vs time for various sampling rates and (b) cartoon of the analyzed disk surface with black sectors representing analyte-painted region.

For the highest sample rate, 75 samples/s, insufficient ion intensity to allow for finer time binning led to poor resolution of individual sample spots. The individual spots are better resolved at 50 samples/s. At this sampling rate, the residence time of each spot is 10 ms, because half the disk is blank, and the linear velocity of the disk at the point of measurement is approximately 3.1 m/s. The rate of 50 samples/s presents a maximum sampling rate 18.7 times greater than the result by Chen et al. of 2.67 samples/s.(Chen, Talaty et al. 2005) To contrast our result, the work by Chen et al. was completed using a linear ion trap mass spectrometer. The conditions for their result may represent more realistic analytical conditions and may better present an upper limit to

practical analysis. However, we believe that our result shows the potential of this method to achieve a higher sampling rate where the analysis conditions are highly controlled. In our system, the analysis of samples by DESI at 50 samples/s is limited by experimental conditions. However, the analyte signal decay is not instantaneous. This is manifested in Figure 9a by intensities being at their baseline value for less than half the time. The time scale on which the signal decays for an analyte spot will place a limit on the maximum achievable sample analysis rate.

At the spectral acquisition rate necessary to study this sample rate, the ion flux is not sufficient to produce high-fidelity chemical images of the disk from a single pass, but the chemical identities of the deposited analytes and their separation in time is recorded. In order to test our hypothesis that ion flux represents the main limitation on sampling rate and imaging reproduction, we simulated a higher ion count rate by co-adding the data that results from multiple rotations. In contrast to pill-by-pill single-pass analysis, this multipass analysis would be amenable to imaging static systems.

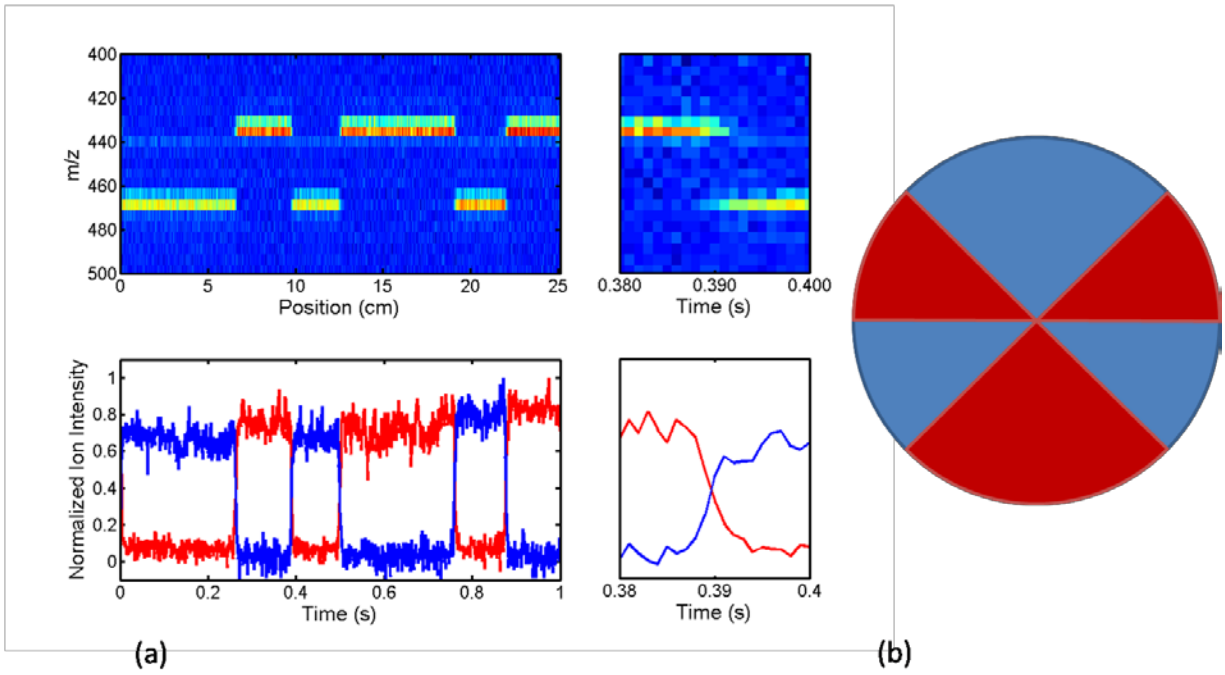

Figure 10: (a) Average of 40 passes of the disk shown in panel b which contains alternating basic blue 7 and rhodamine 6G with unequal sector sizes. The transition region between different analytes is shown in (2) and (4), whereas (1) and (3) are the mass spectra vs time and the resulting analyte signal intensities vs time, respectively.

Figure 10a shows the results from multipass averaging of 40 rotations, over the course of 40 s, of a disk with six sectors of two different sizes, alternating between two analytes. This pattern is shown schematically in Figure 10b. The disk was rotating at 25.1 cm/s with 1 ms time bins used in the figure corresponding to 250 μm on the disk. Plot 1 in Figure 10a shows the reproduction of the pattern drawn on the disk with stable ion intensity for each peak achieved through averaging. The stability of the peak heights suggests that quantitative information is likely extractable if that were the experimental aim. Plot 2 in Figure 10a magnifies one of the regions where the sample switches. The rise/fall times are on the order of 5 ms, which is equivalent to 1.25 mm of translation corresponding to the best approximation of spatial resolution of the experiment for this rotation rate. Physically, this value is only slightly larger than the size of the DESI spray plume on the surface, but the resolution is worse than others have demonstrated. The effective linear imaging rate for this experiment was 6 mm/s.

The present method represents an alternative to rastering a surface to image it and can provide rapid linear imagining rates at a cost to spatial resolution. One advantage of such an imaging process is that it allows for solvent flow rates much higher than those typically used, up to 50 μL/min in these experiments, without blurring the image on the surface. A regularly refreshed surface does not exhibit the same ion current saturation with increased flow rates as seen in previous work on stationary or slow surfaces.(Venter, Sojka et al. 2006) Another advantage stems from reducing the effects of surface capacitance. Previously, different surfaces have been shown to have different effective capacitances.(Volný, Venter et al. 2008) Volný et al. showed surfaces initially exhibit high ion intensity which decays rapidly and to different degrees depending on the surface. Surfaces widely used for DESI suffered less than those generally avoided. They found PTFE to be the best of the tested surfaces, which was explained by its hydrophobicity. In our experiment, the constant rotation of the disk through the DESI plume exploits this period of high ion intensity, providing images more rapidly through higher ion count rates and the co-addition of multiple passes. This finding suggests surfaces not highly amenable to DESI might be better analyzed if repeated measurements are made followed by averaging them together as opposed to one slow scan.

2.4 Studies of Chemical Kinetics

The vision for the use of mass spectrometry as a detector in chemical kinetic experiments on enzymatic systems was first comprehensively summarized in a review by Northrop and Simpson in 1997, after the qualitative mass spectrometric analysis of static biochemical samples had become commonplace worldwide.(Northrop and Simpson 1997) In their key paper, they laid out the potential for the future field where they note that mass spectrometry frees enzymologists from the need to use chromophoric substrates or coupled assays and potentially allows measurements of much lower concentrations of reacting species with higher accuracy and precision. The use of chromophoric substrates presents many challenges to kinetic analysis. In the simplest case, labeling the substrate is a complex or expensive process requiring both reaction and separation steps. More seriously, chemical labels can impact the rate measure and the mechanism of reaction; the reaction must create a change in a spectral feature, and it is often necessary for the chromophore to be intimately involved in the reaction. Thus, the properties of the reaction are affected by an unnatural species at or near the reaction site, rather than a chemical appendage tacked onto a molecule far from the chemically or physically active region. Because mass spectrometers are sensitive to mass-to-charge ratios, chemical labels are not necessary for kinetic analysis. As long as a reaction results in a change in the mass-to-charge ratio of one reagent, or in the case of reactions resulting in structural isomerism, its fragmentation pattern, the product should be detectable using mass spectrometry. Of course, the resolving power of the instrument will always remain a technical limitation. Mass spectrometry is not appropriate for the study of reactions that require the detection of individual enantiomers. In addition to enabling the use of native substrates, a mass spectrometer has the advantage of allowing independent and simultaneous analysis of multiple species provided that they appear at different mass-to-charge ratios. In their review, Northrop and Simpson map out several areas of unique interest for mass spectrometry-based enzyme kinetics: determination of biochemical kinetics, enzyme mechanisms through the detection of intermediates, evaluation of free energy diagrams, determination of diffusion-controlled rate constants, and the independent determination of substrate and product dissociation constants. Northrop and Simpson imagine that in the 21st century the mass spectrometer will replace the spectrophotometer as the principle instrument in the study of the enzymes.

The key requirement of a kinetics experiment is to record a signal's stable value as it changes over time. The measure of relative height or peak area stability is the peak height precision as defined earlier. HT-TOFMS has a peak height precision advantage over traditional, on-axis TOFMS given by Equation 4. Data acquisition over the large mass-to-charge ratio window of a TOF experiment gives MS-based kinetic analysis the capability to monitor the evolution of complex reactions. As shown in Figure 3, HT-TOFMS offers a PHP advantage when compared to traditional TOFMS at any time scale. The PHP enhancement is most pronounced for spectra collected on shorter time scales with less signal averaging that are relevant to kinetic studies. Thus, HT-TOFMS potentially provides an ideal experimental tool for the mass spectrometric analysis of chemical reactions.

A stopped-flow kinetics apparatus that uses HT-TOFMS as a detector has been constructed from commercially available components. The device consists of two syringes that can be rapidly driven using a high-pressure syringe pump (PhD 2000, Harvard Apparatus, Holliston, MA) to produce a total flow rate from the syringes of 1-3 mL per second. The flow from the two syringes is mixed using a Berger-Ball mixer (Olis Incorporated, Bogart, GA) and the output is used to fill a sample loop on a multi-way, two state valve.(Berger, Balko et al. 1968) The flow path for liquid in the valve during the sample loop filling state is shown in Figure 11(left) and the flow path for the analysis state is shown in Figure 11(right). In this stopped-flow configuration a 50 μL sample loop and the associated flow path can be filled in approximately 60 ms using the syringe pump. The sample loop and all tubing are constructed from .030" PEEK. The use of the large, .030" fluidic components is necessitated by the pressure limitation of the syringe pump. The use of smaller diameter tubing would reduce the minimum delay before the first time point is analyzed, also known as the sample dead-time. The valve used has an 80 PSI helium-driven pneumatic actuator (C2H-200A, VICI Valco, Inc, Houston, Texas) that when controlled using an available accessory (HSSI, VICI Valco) for 80 PSI nitrogen pilot valve actuation can switch between states in less than in 10 ms.(Harvey, Robinson et al. 1994) This pneumatic valve is the fastest actuating two-state valve currently on the market.

Using this system, a total dead time—the time between mixing the two reagents and the first reaction data point collected by the mass spectrometer—of approximately 100 milliseconds can be achieved by using a high ESI flow rate to direct the output of the valve into the mass spectrometer. The liquid flow for ESI in the apparatus is provided by an HPLC pump (AD-10,

Shimadzu Scientific Instruments, Columbia, MD). The HPLC pump provides a more stable flow rate than a syringe pump used in the same configuration. Additionally, the HPLC pump can provide the higher backing pressure necessary for high flow rate ESI through a narrow ESI emitter. In this design the maximum observation time is limited by the volume of the sample loop, the minimum swept volume, and the rate of analyte flow to the ESI emitter. The sample observation time—the amount of time needed to fully deplete the contents of the sample loop—is coupled to the point of earliest analysis, which is reduced by using a higher ESI flow rate.

The valve used has been modified to reduce its contribution to the dead-time of the experiment and minimize its swept volume during the inject state. While most of the through holes in the stator are 0.030", and match the diameter of the PEEK sample loop, the through hole for the ESI emitter port has been reduced to 0.010". This reduction in diameter addresses what was the largest contribution in the prototype apparatus to the dead-time in the experiment. Because the ESI emitter port is never directly connected to the output of the mixer, this reduction in diameter is not controlled by the pressure limitations of the syringe pump.

To follow the path of the liquid in the system described in Figure 11, in the load phase a 3 mL pulse of two reactant solutions are forced through a Berger ball mixer at a 1-3 mL/s flow rate using a high pressure syringe pump. After exiting the mixer, the reaction solution fills a sample loop on a six-way, two state pneumatically actuated valve. While the sample loop is filled, stable nebulization-assisted electrospray is maintained by the continuous flow of a tracer solution in the same solvent as the reacting species. The tracer solution is composed of the same solvent system as the analyte and contains at least one compound that can be monitored by mass spectrometry during the period before and after a stopped-flow kinetic measurement.

The load phase is terminated by the actuation of the pneumatic valve which is designed to switch in less than 10 ms.(Harvey, Robinson et al. 1994) After the valve switch the flow is directed so that the reacting solution in the sample loop is pushed to the electrospray tip where the reaction is quenched by solvent evaporation and the reaction progress can be analyzed by the mass spectrometer. Analysis dead time and reaction observation time is a function of sample loop volume and electrospray flow rate. The valve switch results in the output of a TTL pulse that is transformed into a NIM pulse with a 10 μs delay using a delay generator. The time of the NIM pulse is recorded using the same time-to-digital convertor that is used to analyze the data

from the delay-line anode. During analysis of kinetic data, the time of this switch trigger pulse is used as the primary reference time.

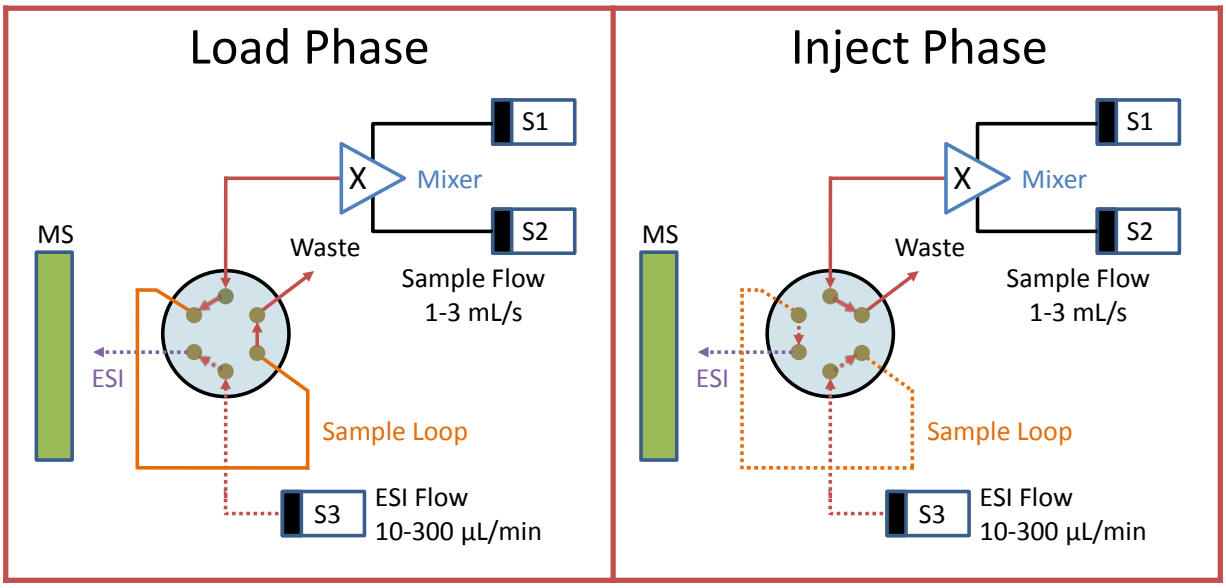

Figure 11: (Left) Flow path diagram of the stopped-flow apparatus in the load phase during which the two reagent solutions mix and fill a sample loop. (Right) Flow path diagram of the stopped-flow apparatus in the inject phase, when the reaction occurring in the sample loop volume is monitored by ESI HT-TOFMS.

In order to test the stopped-flow system on a well-studied chromophoric system before exploring the hydrolysis of unlabeled peptides whose kinetics are unknown, the hydrolysis of BPVApNA (Sigma Aldrich) by trypsin (proteomics grade, Sigma Aldrich) was performed. BPVApNA is an acronym that will be used in this work for N-benzoyl-L-phenylalanyl-L-valyl-L-arginine-4-nitroanaline, a chromophoric artificial trypsin substrate. Trypsin is a proteolytic enzyme that is selective for the hydrolysis of the amide bond at the carboxylic acid side of arginine and lysine sites on proteins and polypeptides. The stopped-flow apparatus shown in Figure 11 was modified for this work by the addition of a microfluidic mixer that was used to acidify the reaction solution before ESI analysis at the mass spectrometer.(Xu, Bessoth et al. 2000) Acidification occurs milliseconds before the reaction is analyzed. Addition of acid quenches the activity of trypsin, which is inactive below pH 6, and increases the sensitivity of ESI for basic analytes.

The results of the stopped-flow HT-TOFMS analysis of BPVApNA at pH 8.5, triethylammonium bicarbonate buffer, are presented in Figure 13 along with the results of optical

stopped-flow analysis and corresponding literature values. A concentration calibration curve for this experiment was extracted from the first second of data collection from the series of substrate concentrations studied. The stead-state hydrolysis rates for the different substrate concentrations were determined using the method of initial rate fitting. The values of K_m and k_{cat} for the system presented in Figure 13 were determined by direct fitting of the initial rates data to the Michaelis-Menten equation. Excellent agreement is shown amongst the values indicating that the stopped-flow HT-TOFMS system is an effective tool to evaluate the steady-state kinetics parameters of certain enzymatic systems. All systems were studied at the uncontrolled room temperature of 22.5 ± 1°C. The literature values presented in Figure 13 were collected at 25°C.

After verification of the stopped-flow MS apparatus on a chromophoric system, the device was applied to the study of the hydrolysis of two unlabeled polypeptides by trypsin. The peptides VGVRVR (American Peptide, Inc., Sunnyvale, CA) and VGVKVR (GenScript USA, Inc., Piscataway, NJ) were selected to allow comparison of the kinetic parameters for two polypeptides that vary only in their active residue. Additionally, these particular sequences were selected because trypsin prefers an amino acid sequence with an aliphatic species in the P_1' site and hydrolyzes them at a faster rate.(Kurth, Grahn et al. 1998) Because neither VGVXVR or its hydrolytic products strongly interact with visible light, these systems cannot be studied using traditional photometric stopped-flow analysis.

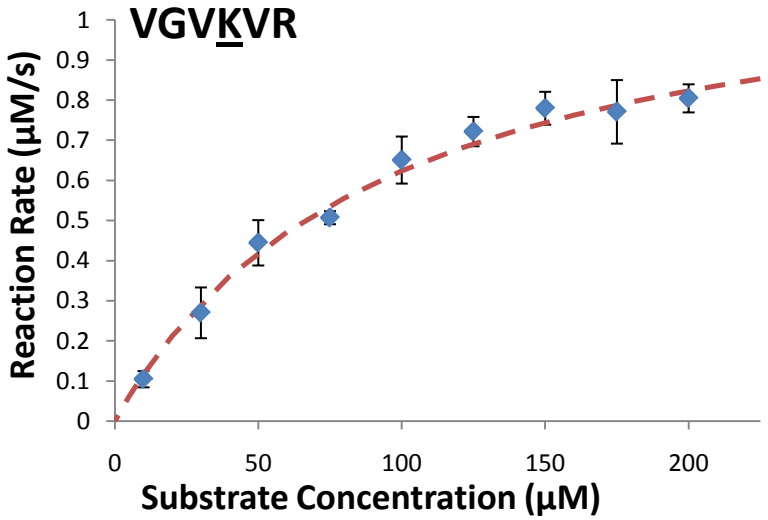

Figure 12: Steady-state hydrolysis of VGVKVR hexapeptide over the concentration range of 10-200 µM by trypsin analyzed using stopped-flow HT-TOFMS.

Figure 12 shows the result initial-rate analysis of the steady-state hydrolysis of VGVKVR by trypsin at pH 8.5. The dashed red line in the figure shows a best fit to the Michaelis-Menten equation for the data collected. The error bars in the figure represent the standard deviation for three experiments collected on three different days. The average standard deviation is less than ten percent of the measured value. This level of error is considered acceptable for a biochemical kinetic measurement.

Substrate	$k_{cat}(s^{-1})$	$K_m(\mu M)$
VGVRVR (MS)	15 ± 1	60 ± 10
VGVKVR (MS)	6.4 ± 0.4	93 ± 13
DABCYL-GPARLAIG-EDANS (F) [2]	40 ± 2.5	34 ± 3
DABCYL-GPAKLAIG-EDANS (F) [2]	10 ± 1	58 ± 5
Tos-GPR-AMC (UV-Vis) [2]	94 ± 2	14 ± 1
Tos-GPK-AMC (UV-Vis) [2]	49 ± 0.1	37 ± 2
BPVApNA (UV-Vis) [1]	28 ± 1.4	38 ± 4
BPVApNA (UV-Vis)	32 ± 2.4	53 ± 9
BPVApNA (MS)	27 + 1.2	36 ± 5

Figure 13: Comparison of the steady-state hydrolysis kinetics of amide substrate species by trypsin using stopped-flow UV-Vis spectrophotometry, stopped-flow fluorescence (F) or stopped-flow HT-TOFMS (MS). [1](Lottenberg, Christensen et al. 1981) [2](Grahn, Ullmann et al. 1998)

The comparison values for relative K/R hydrolysis in Figure 13 are from two different classes of experiments. The DABCYL-XXX-EDANS experiments are based on florescence resonance energy transfer (FRET) that causes quenching of the fluorescent emission on one of the fluorescent labels. In FRET experiments, a fluorescent donor moiety can transfer energy to another fluorescent moiety in the same molecule through dipole-dipole coupling, provided that the moieties are proximate and that the emission spectrum of the donor overlaps with the excitation spectrum of the acceptor moiety.(Stryer 1978) This energy transfer is efficient over distances of approximately 100 Å and cleavage of the polypeptide chain results in a substantial increase in fluorescent emission from the donor species (40X).(Matayoshi, Wang et al. 1990) In this work, DABCYL [4-(4-dimethylaminophenylazo)benzoic acid] serves as the quenching acceptor and EDANS [5-[(2-aminoethyl)amino]naphthalene-1-sulfonic acid] as the donor. The DABCYL-EDANS motif has been used for a number of peptide hydrolysis studies. Other

donor-acceptor FRET pairs have also been used to label peptides for kinetic analysis.(Geoghegan 1996)

In addition to a maximum accessible donor-acceptor separation, the FRET quenching method does have some limitations when applied to the study of enzyme kinetics. One limitation is that the interaction of the fluorophores with the enzyme may impact the measured kinetic values. An additional consideration is that addition of the fluorophores may impact the solubility of the sample. Also, the complexity of the selective labeling chemistry increases the effort or cost involved in preparation of the substrate. The most significant consideration, however, is the limited applicability of the analytical procedure to reactions with higher substrate concentrations (> 20 μM) due to the inner-filter effect (IFE).(Holskin, Bukhtiyarova et al. 1995; Geoghegan 1996) The IFE is the effect of decreased detected fluorescent emission due to absorption by other fluorophores and results in a non-linear relationship between concentration and fluorescence intensity. Correction methods exist to overcome IFE limitations, but represent a challenge for expanding FRET methods for online kinetic analysis.(Palmier and Van Doren 2007)

The Tos-GPX-AMC values represent kinetic values for the hydrolysis of artificial amide substrates where GPX designation corresponds to a sequence of three amino acids where the third residue is either lysine or arginine. AMC is an acronym for 7-amino 4-methyl coumarin, a fluorophore whose hydrolysis can be monitored by changes in its spectral signature. In all three cases the relative reactivity and selectivity for arginine over lysine is preserved

The experimental method of stopped-flow HT-TOFMS was validated by comparing the optical and mass spectrometric stopped-flow analysis of a chromophoric artificial trypsin substrate. Two new native polypeptide samples, for which no kinetic values for trypsin hydrolysis were available in the literature, were studied. This work shows the potential to use HT-TOFMS as a detector for a stopped-flow kinetics experiment.

2.4 References

Berger, R. L., B. Balko, et al. (1968). "High Resolution Mixer for the Study of the Kinetics of Rapid Reactions in Solution." Review of Scientific Instruments **39**(4): 493-498.

Brenton, A. G., T. Krastev, et al. (2007). "Improvement of the duty cycle of an orthogonal acceleration time-of-flight mass spectrometer using ion gates." Rapid Communications in Mass Spectrometry **21**(18): 3093-3102.

Chen, H., N. N. Talaty, et al. (2005). "Desorption Electrospray Ionization Mass Spectrometry for High-Throughput Analysis of Pharmaceutical Samples in the Ambient Environment." Analytical Chemistry **77**(21): 6915-6927.

Cooks, R. G., J. H. Beynon, et al. (1973). Metastable Ions. Amsterdam, Elsevier Scientific Publishing Company.

de Maaijer-Gielbert, J., J. H. M. Beijersbergen, et al. (1996). "Surface-induced dissociation of benzene on a PFPE liquid insulator in a time-of-flight mass spectrometer." International Journal of Mass Spectrometry and Ion Processes **153**(2-3): 119-128.

Dongré, A. R., Á. Somogyi, et al. (1996). "Surface-induced Dissociation: An Effective Tool to Probe Structure, Energetics and Fragmentation Mechanisms of Protonated Peptides." Journal of Mass Spectrometry **31**(4): 339-350.

Falick, A. M., W. M. Hines, et al. (1993). "Low-mass ions produced from peptides by high-energy collision-induced dissociation in tandem mass spectrometry." Journal of the American Society for Mass Spectrometry **4**(11): 882-893.

Fenn, J. B. and M. Mann (1989). "Electrospray ionization for mass spectrometry of large biomolecules." Science **246**(4926): 64-72.

Galhena, A. S., S. Dagan, et al. (2008). "Surface-Induced Dissociation of Peptides and Protein Complexes in a Quadrupole/Time-of-Flight Mass Spectrometer." Analytical Chemistry **80**(5): 1425-1436.

Gamage, C. M., F. M. Fernandez, et al. (2004). "Submicrosecond Surface-Induced Dissociation of Peptide Ions in a MALDI TOF MS." Analytical Chemistry **76**(17): 5080-5091.

Geoghegan, K. F. (1996). "Improved Method for Converting an Unmodified Peptide to an Energy-Transfer Substrate for a Proteinase." Bioconjugate Chemistry **7**(3): 385-391.

Grahn, S., D. Ullmann, et al. (1998). "Design and Sythesis of Fluorogenic Trypsin Peptide Substrates Based on Resonance Energy Transfer." Analytical Biochemistry **265**: 225-231.

Haney, L. L. and D. E. Riederer (1999). "Delayed extraction for improved resolution of ion/surface collision products by time-of-flight mass spectrometry." Analytica Chimica Acta **397**(1-3): 225-233.

Harvey, M. C., R. E. Robinson, et al. (1994). "Further Studies on High-Speed Switching of Chromatographic Valves." Journal of Chromatographic Science **32**: 190-194.

Holskin, B. P., M. Bukhtiyarova, et al. (1995). "A Continuous Fluorescence-Based Assay of Human Cytomegalovirus Protease Using a Peptide Substrate." Analytical Biochemistry **227**(1): 148-155.

Hutchens, T. W. and T. T. Yip (1993). "New desorption strategies for the mass spectrometric analysis of macromolecules." Rapid Communications in Mass Spectrometry **7**(7): 576-580.

Ifa, D. R., J. M. Wiseman, et al. (2007). "Development of capabilities for imaging mass spectrometry under ambient conditions with desorption electrospray ionization (DESI)." International Journal of Mass Spectrometry **259**(1-3): 8-15.

Ioannis, A. P. (1995). "The interpretation of collision-induced dissociation tandem mass spectra of peptides." Mass Spectrometry Reviews **14**(1): 49-73.

Kaufmann, R., D. Kirsch, et al. (1994). "Sequenching of peptides in a time-of-flight mass spectrometer: evaluation of postsource decay following matrix-assisted laser desorption ionisation (MALDI)." International Journal of Mass Spectrometry and Ion Processes **131**: 355-385.

Kimmel, J. R. (2004). Continuous, Multiplexed Time-of-Flight Mass Spectrometry of Electrosprayed Ions. Chemistry. Stanford, Stanford University. **PhD**.

Kimmel, J. R., O. K. Yoon, et al. (2005). "Peak Height Precision in Hadamard Transform Time-of-Flight Mass Spectra." Journal of the American Society for Mass Spectrometry **16**(7): 14p.

Kurth, T., S. Grahn, et al. (1998). "Engineering the S1' Subsite of Trypsin: Design of a Protease Which Cleaves between Dibasic Residues." Biochemistry **37**(33): 11434-11440.

Laskin, J. and C. Lifshitz (2001). "Kinetic energy release distributions in mass spectrometry." Journal of Mass Spectrometry **36**(5): 459-478.

Lottenberg, R., U. Christensen, et al. (1981). "Assay of Coagulation Proteases Using Peptide Chromogenic and Fluorogenic Substrates." Methods in Enzymology **80**.

Matayoshi, E. D., G. T. Wang, et al. (1990). "Novel fluorogenic substrates for assaying retroviral proteases by resonance energy transfer." Science **247**(4945): 954-958.

Morris, M. R., D. E. Riederer, et al. (1992). "Ion/surface collisions at functionalized self-assembled monolayer surfaces." International Journal of Mass Spectrometry and Ion Processes **122**: 181-217.

Northrop, D. B. and F. B. Simpson (1997). "New concepts in bioorganic chemistry beyond enzyme kinetics: Direct determination of mechanisms by stopped-flow mass spectrometry." Bioorganic & Medicinal Chemistry **5**(4): 641-644.

Paizs, B. and S. Suhai (2005). "Fragmentation pathways of protonated peptides." Mass Spectrometry Reviews **24**(4): 508-548.

Palmier, M. O. and S. R. Van Doren (2007). "Rapid determination of enzyme kinetics from fluorescence: Overcoming the inner filter effect." Analytical Biochemistry **371**(1): 43-51.

Roepstorff, P. and J. Fohlman (1984). "Letter to the editors." Biological Mass Spectrometry **11**(11): 601.

Schey, K., R. G. Cooks, et al. (1987). "A tandem time-of-flight mass spectrometer for surface-induced dissociation." International Journal of Mass Spectrometry and Ion Processes **77**(1): 49-61.

Schey, K. L., R. Graham Cooks, et al. (1989). "Ion/surface collision phenomena in an improved tandem time-of-flight instrument." International Journal of Mass Spectrometry and Ion Processes **94**(1-2): 1-14.

Spencer, M. K., M. R. Hammond, et al. (2008). "Laser mass spectrometric detection of extraterrestrial aromatic molecules: Mini-review and examination of pulsed heating effects." Proceedings of the National Academy of Sciences **105**(47): 18096-18101.

Stryer, L. (1978). "Fluorescence Energy Transfer as a Spectroscopic Ruler." Annual Review of Biochemistry **47**(1): 819-846.

Tanaka, K., H. Waki, et al. (1988). "Protein and polymer analyses up to m/z 100 000 by laser ionization time-of-flight mass spectrometry." Rapid Communications in Mass Spectrometry **2**(8): 151-153.

Venter, A., P. E. Sojka, et al. (2006). "Droplet Dynamics and Ionization Mechanisms in Desorption Electrospray Ionization Mass Spectrometry." Analytical Chemistry **78**(24): 8549-8555.

Volný, M., A. Venter, et al. (2008). "Surface effects and electrochemical cell capacitance in desorption electrospray ionization." Analyst **133**: 525-531.

Williams, E. R., L. Fang, et al. (1993). "Surface induced dissociation for tandem time-of-flight mass spectrometry." International Journal of Mass Spectrometry and Ion Processes **123**(3): 233-241.

Williams, E. R., G. C. Jones, et al. (1992). "Ion pickup of large, surface-adsorbed molecules: a demonstration of the Eley-Rideal mechanism." Journal of the American Chemical Society **114**(9): 3207-3210.

Wysocki, V. H., J.-M. Ding, et al. (1992). "Surface-induced dissociation in tandem quadrupole mass spectrometers: A comparison of three designs." Journal of the American Society for Mass Spectrometry **3**(1): 27-32.

Xu, Y., F. G. Bessoth, et al. (2000). "On-line monitoring of chromium(III) using a fast micromachined mixer/reactor and chemiluminescence detection " The Analyst **125**: 677-683.

Yoon, O. K., I. A. Zuleta, et al. (2007). "Simple Template-Based Method to Produce Bradbury-Nielsen Gates." Journal of the American Society for Mass Spectrometry **18**(11): 1901-1908.

Zuleta, I. A., G. K. Barbula, et al. (2007). "Micromachined Bradbury-Nielsen Gates." Analytical Chemistry **79**(23): 9160-9165.

3. Personnel Supported

Richard N. Zare, Principal Investigator

Oh Kyu Yoon, Graduate Student

Matthew D. Robbins, Graduate Student

Griffin Barbula, Graduate Student

David Leahy, Research Associate

4. Publications

4.1 Refereed Publications

G. K. Barbula, M. D. Robbins, O. K. Yoon, I. Zuleta, and R. N. Zare, "Desorption Electrospray Ionization: Achieving Rapid Sampling Rates," *Anal. Chem.* (in press).

O. K. Yoon, M. D. Robbins, I. Zuleta, G. Barbula, and R. N. Zare, "Continuous Time-of-Flight Ion Imaging: Application to Fragmentation," *Anal. Chem.* **80**, 8299-8306 (2008).

M. D. Robbins, O. K. Yoon, I. A. Zuleta, G. K. Barbula, and R. N. Zare, "Computer-Controlled, Variable-Frequency Power Supply for Driving Multipole Ion Guides," *Rev. Sci. Instrum.* **79**, 034702 (2008).

I. A. Zuleta, G. K. Barbula, M. D. Robbins, O. K. Yoon, and R. N. Zare, "Micromachined Bradbury-Nielsen Gates," *Anal. Chem.* **79**, 9160-9165 (2007).

O. K. Yoon, I. A. Zuleta, M. D. Robbins, G. K. Barbula, and R. N. Zare, "Simple Template-Based Method to Produce Bradbury-Nielsen Gates," *J. Am. Soc. Mass Spectrom.* **18**, 1901-1908 (2007).

4.2 Doctoral Theses

O. K. Yoon. "Continuous Time-of-Flight Mass Spectrometric Imaging of Fragmented Ions" Stanford University, Stanford, CA, October 2009.

M. D. Robbins. "Stopped-Flow Chemical Kinetic Analysis Using Imaging Hadamard Transform Mass Spectrometry" Stanford University, Stanford, CA, October 2009.

5. Inventions

5.1 Patents Awarded

O. K. Yoon, R. N. Zare, "Method of making gate for charged particle motion " U.S. Patent 7,448,131, November 11, 2008.

5.2 Patents Pending

O. K. Yoon, R. N. Zare, "Fragmentation modulation mass spectrometry " Filed 2008.

6. Presentations

Poster Presentation: Barbula, G. K.; Robbins, M. D.; Zare, R. N.; “Rapid Desorption Electrospray Ionization Using Hadamard Transform Time-of-Flight Mass Spectrometry.” American Society of Mass Spectrometry Conference. 2009.

Poster Presentation: Robbins, M. D.; Barbula, G. K.; Zare, R. N.; “Stopped-Flow Biochemical Kinetics Analyzed by Hadamard Transform Time-of-Flight Mass Spectrometry .” American Society of Mass Spectrometry Conference. 2009.

Poster Presentation: Robbins, M. D.; Barbula, G. K.; Zare, R. N.; “Kinetic Studies of Reactions in Solution Using Fast Mass Spectrometry: Stopped-Flow Hadamard Transform Time-of-Flight.” AFOSR Molecular Dynamics Meeting. 2009.

Poster Presentation: Yoon, O. K.; Robbins, M. D.; Zuleta, I. A.; Barbula, G. K.; Zare, R. N.; “Continuous Time-of-Flight Mass Spectrometer Based on Ion Modulation, Ion Imaging, and Kinetic Energy Analysis.” American Society of Mass Spectrometry Conference. 2008.

Poster Presentation: Zuleta, I. A.; Yoon, O. K.; Robbins, M. D.; Barbula, G. K.; Zare, R. N.; “What is the speed limit of ESI? Simulation, measurement and analysis of long nanoESI-HT-TOFMS time traces of some relevant fast processes.” American Society of Mass Spectrometry Conference. 2007.

Oral Presentation: Zare, R. N.; Barbula, G. K.; Robbins, M. D.; Yoon, O. K., Zuleta, I. A.; “Hadamard Transform Time-of-Flight Mass Spectrometry” AFOSR Molecular Dynamics Meeting. 2007.

Oral Presentation: Yoon, O. K.; Robbins, M. D.; “Time-of-Flight Mass Spectrometer Based on Ion Modulation and Ion Imaging” Edwards Air Force Base. 2007.

Poster Presentation: Yoon, O. K.; Zuleta, I. A.; Robbins, M. D.; Barbula, G. K.; Zare, R. N.; “Ion Modulation and Noise in Hadamard Transform Time-of-Flight Mass Spectrometry – How fast or slow can you acquire mass spectra?” ACS National Meeting. 2007.